METABOLIC DISEASE

Neuropilin-1 expression in adipose tissue macrophages protects against obesity and metabolic syndrome

Ariel Molly Wilson,[1,2] Zhuo Shao,[1] Vanessa Grenier,[1] Gaëlle Mawambo,[1] Jean-François Daudelin,[3] Agnieszka Dejda,[1,4] Frédérique Pilon,[4] Natalija Popovic,[4] Salix Boulet,[3] Célia Parinot,[1] Malika Oubaha,[1] Nathalie Labrecque,[3] Vincent de Guire,[1] Mathieu Laplante,[5] Guillaume Lettre,[6] Florian Sennlaub,[7] Jean-Sebastien Joyal,[8] Michel Meunier,[2] Przemyslaw Sapieha[1,4]*

Obesity gives rise to metabolic complications by mechanisms that are poorly understood. Although chronic inflammatory signaling in adipose tissue is typically associated with metabolic deficiencies linked to excessive weight gain, we identified a subset of neuropilin-1 (NRP1)–expressing myeloid cells that accumulate in adipose tissue and protect against obesity and metabolic syndrome. Ablation of NRP1 in macrophages compromised lipid uptake in these cells, which reduced substrates for fatty acid β-oxidation and shifted energy metabolism of these macrophages toward a more inflammatory glycolytic metabolism. Conditional deletion of NRP1 in LysM Cre-expressing cells leads to inadequate adipose vascularization, accelerated weight gain, and reduced insulin sensitivity even independent of weight gain. Transfer of NRP1$^+$ hematopoietic cells improved glucose homeostasis, resulting in the reversal of a prediabetic phenotype. Our findings suggest a pivotal role for adipose tissue–resident NRP1$^+$-expressing macrophages in driving healthy weight gain and maintaining glucose tolerance.

INTRODUCTION

Obesity and its ensuing sequelae of metabolic syndrome, type 2 diabetes mellitus, and cardiovascular complications are in global pandemic (*1*). During weight gain in response to excessive caloric intake, lipid overload in adipose tissue triggers classical macrophage polarization, cytokine release, systemic inflammation, local proliferation of adipose tissue macrophages (ATMs), and infiltration of circulating monocytes, which in concert are believed to contribute to systemic complications such as insulin resistance (*2*–*5*). This has led to a generalized association between inflammation, macrophage activation, and the pathogenesis of metabolic diseases (*6*). Yet, subsets of ATMs have also been suggested to participate in lipid trafficking within adipose tissue (*7*), and adipose tissue inflammation itself has been proposed to be an adaptive response permitting effective storage of excess nutrients (*8*). These divergent views on adipose tissue inflammation highlight the need to tease out the characteristics of both beneficial and detrimental inflammatory processes during weight gain.

Protective adipose inflammation may be necessary for adequate tissue plasticity and angiogenesis given the role of mononuclear phagocytes in tissue remodeling and vascular growth (*9*, *10*). Fat pads necessitate a stable and dynamic vascular plexus to couple metabolic supply to adipocyte demands during hypertrophy and hyperplasia; thus, angiogenesis has been proposed to be a prerequisite for adipose tissue expansion (*11*). Adipose vasculature also plays a key role in fatty acid (FA) transport from circulation in part through vascular endothelial growth factor B (VEGF-B)–induced FATP3 up-regulation (*12*). Binding of VEGF-B to VEGF receptor 1 (VEGFR1) and its co-receptor neuropilin-1 (NRP1) increases endothelial lipid uptake. NRP1 is a multiligand single-pass transmembrane receptor originally identified as an adhesion molecule and later as a receptor for neuronal guidance cues. NRP1 is now also well recognized for its roles in angiogenesis and maintenance of vessel integrity (*13*–*15*). Monocytes/macrophages expressing NRP1 are proangiogenic and facilitate neovascularization in the mature central nervous system (CNS) and in tumors (*16*, *17*). Given the roles of NRP1 in angiogenesis (*14*, *15*), lipid uptake (*12*), and the propensity of NRP1$^+$ macrophages to promote vascularization (*16*, *17*), we investigated the implication of NRP1-expressing myeloid cells in obesity.

Here, we show that NRP1-expressing ATMs are critical mediators of protective inflammation during weight gain. Our data reveal that within the myeloid lineage, NRP1 is most abundantly expressed by ATMs where it regulates FA availability for β-oxidation. ATMs devoid of NRP1 are less efficient at internalizing lipids and shift their metabolism toward carbohydrate-based glycolysis. As a consequence of their dependence on glycolysis, NRP1-deficient macrophages take on a proinflammatory M1-like phenotype, further contributing to metabolic dysfunction. Ultimately, NRP1-expressing myeloid cells influence glucose tolerance and insulin sensitivity, even before excessive weight gain.

RESULTS

NRP1-expressing macrophages accumulate in adipose tissue during diet-induced obesity

We investigated expression profiles of *Nrp1* in myeloid cells with data from the immunological consortium ImmGen (Immunological Genome Project) (*18*). *Nrp1* was robustly expressed in ATMs compared

[1]Department of Biochemistry, Maisonneuve-Rosemont Hospital Research Centre, University of Montreal, Montreal, Quebec H1T 2M4, Canada. [2]Department of Engineering Physics, École Polytechnique de Montréal, Montreal, Quebec H3T 1J4, Canada. [3]Department of Microbiology, Infectiology and Immunology, Maisonneuve-Rosemont Hospital Research Centre, University of Montreal, Montreal, Quebec H1T 2M4, Canada. [4]Department of Ophthalmology, Maisonneuve-Rosemont Hospital Research Centre, University of Montreal, Montreal, Quebec H1T 2M4, Canada. [5]Centre de recherche de l'Institut universitaire de cardiologie et de pneumologie de Québec (CRIUCPQ), Université Laval, Faculté de médecine, 2725 Chemin Ste-Foy, Quebec, Quebec G1V 4G5, Canada. [6]Montreal Heart Institute, Université de Montréal, Montreal, Quebec H1T 1C8, Canada. [7]Institut de la Vision, Institut National de la Santé et de la Recherche Médicale, U 968, Paris F-75012, France. [8]Departments of Pediatrics, Ophthalmology, and Pharmacology, Centre Hospitalier Universitaire Ste-Justine Research Center, Université de Montréal, Montreal, Quebec H1T 2M4, Canada.
*Corresponding author. Email: mike.sapieha@umontreal.ca

with other steady-state tissue-resident macrophages, monocytes, and neutrophils (Fig. 1A). These data pointed to a potential role of NRP1$^+$ macrophages in adipose tissue homeostasis.

We therefore placed adult (8-week-old) C57BL/6 mice on high-fat diet (HFD) (59% fat calories) for 10 weeks, investigated ATM populations by fluorescence-activated cell sorting (FACS), and kept age-matched controls for the same duration on regular diet [normal chow diet (NCD); 18% fat calories]. All ATMs in this study were collected from visceral white adipose tissue (VAT) located in the peritoneal cavity. In accordance with other studies, an increase in ATMs was detected in adipose tissue of HFD-fed mice when compared with age-matched controls on NCD (fig. S1A). This was paralleled by a proportionate increase in NRP1$^+$ ATMs (Fig. 1B). However, there was no change in numbers of systemic, circulating NRP1$^+$ monocytes, nor was their surface expression of NRP1 [mean fluorescence intensity (MFI)] detected after 4 weeks of HFD when compared with NCD (Fig. 1C). This suggests that circulating monocytes do not up-regulate NRP1 at the onset of obesity, and there is a selective accretion of NRP1$^+$ ATMs in the adipose tissue of HFD-fed mice.

Given that NRP1 is expressed by multiple cell types including immune cells (*19*), blood vessels (*20*), and neurons (*21*), we next unbiasedly localized NRP1 in expanding adipose tissue. Immunohistochemistry on VAT in both mice fed HFD for 10 weeks and age-matched NCD mice (fig. S1B) confirmed robust NRP1 expression on F4/80$^+$ macrophages (white arrows) at the periphery of perilipin-labeled adipocytes, as well as lectin-stained blood vessels. To confirm myeloid expression of NRP1 in VAT, we generated the LysM-Cre/ROSAEYFP$^{fl/fl}$ myeloid reporter mouse that endogenously expresses yellow fluorescent protein (YFP) in myeloid lineage cells (*22*). After 22 weeks of HFD, NRP1 localized predominantly to crown-like structures (CLSs) (white arrowheads), which correspond to agglomerations of phagocytic macrophages surrounding dying and dead adipocytes (Fig. 1D, left) (*23*). High-magnification 4′,6-diamidino-2-phenylindole (DAPI) staining confirmed that the YFP$^+$ macrophage signal corresponds to clusters of cells (Fig. 1D, bottom). Together, these data demonstrate robust expression of NRP1 in ATMs and suggest accretion of NRP1$^+$ macrophages in adipose tissue during HFD-induced weight gain.

NRP1-expressing myeloid cells regulate diet-induced weight gain and glucose tolerance

To elucidate the role of NRP1$^+$ macrophages in adipose tissue homeostasis and weight gain, we generated a LysM-CRE-*Nrp1*$^{fl/fl}$ mouse line with NRP1 ablated in cells of myeloid lineage (*17*). Deletion of NRP1 in LysM-Cre-*Nrp1*$^{fl/fl}$ ATMs was confirmed by FACS (Fig. 1E). LysM-Cre-*Nrp1*$^{fl/fl}$ and its transgenic control LysM-Cre-*Nrp1*$^{+/+}$ or wild-type (WT) mice were fed either NCD or HFD, and weight gain was monitored. When fed NCD, LysM-Cre-*Nrp1*$^{fl/fl}$ mice had similar weight gain profiles to the controls (Fig. 1F); EchoMRI scans confirmed no significant differences in lean mass or body fat composition, and dual-energy x-ray absorptiometry (DEXA) scan detected similar bone density (Fig. 1F and fig. S1E). Although weight gain was similar between LysM-Cre-*Nrp1*$^{+/+}$ and LysM-Cre-*Nrp1*$^{fl/fl}$ mice fed NCD, the latter already presented with glucose intolerance and decreased insulin sensitivity (Fig. 1G).

However, when mice were placed on HFD, LysM-Cre-*Nrp1*$^{fl/fl}$ mice gained significantly more weight than LysM-Cre-*Nrp1*$^{+/+}$ mice (Fig. 1H). EchoMRI scans confirmed that weight gain in LysM-Cre-*Nrp1*$^{fl/fl}$ mice stems from fat mass increase and not gains in lean mass, and DEXA scans revealed equal bone density (Fig. 1H and fig. S1F). The observed glucose intolerance and decreased insulin sensitivity in LysM-Cre-*Nrp1*$^{fl/fl}$ mice on NCD were exacerbated by HFD (Fig. 1I) and persisted even at a time point of 16 weeks when weight gain had plateaued and there was no longer any weight discrepancy between LysM-Cre-*Nrp1*$^{+/+}$ and LysM-Cre-*Nrp1*$^{fl/fl}$ mice (Fig. 1H).

NRP1-expressing myeloid cells influence adipocyte hypertrophy, fatty liver, and CLS formation

The increased fat mass phenotype observed in LysM-Cre-*Nrp1*$^{fl/fl}$ mice led us to characterize their adipose tissue by immunohistochemistry. We first labeled adipocyte membranes with perilipin (Fig. 2A) and noted significant enlargement of adipocytes in LysM-Cre-*Nrp1*$^{fl/fl}$ mice and a proportional reduction of adipocyte numbers per area after 10 weeks of HFD. Hypertrophic visceral adipocytes are more lipolytic (*24*, *25*), leading to increased free FA release into the portal vein (*26*), which augments the risk of fatty liver. We therefore isolated livers from control and LysM-Cre-*Nrp1*$^{fl/fl}$ mice after 10 weeks of HFD and found that mice with deficiency in myeloid NRP1 had larger, heavier livers (Fig. 2B) with larger clusters of lipid droplets (Fig. 2C). In addition to fatty livers, adipocyte hypertrophy also leads to adipocyte necrosis and recruitment of macrophages to form CLS (*23*). We observed a significant rise in CLS in LysM-Cre-*Nrp1*$^{fl/fl}$ VAT when compared with controls (Fig. 2D). These data corroborate that myeloid deficiency in NRP1 results in hypertrophic and degenerating adipose tissue, in addition to nonalcoholic fatty liver.

NRP1-expressing myeloid cells contribute to adipose tissue vascularization

Expanding adipocytes require concomitant vascular network growth to maintain oxygen and trophic support. The adipose phenotype of LysM-Cre-*Nrp1*$^{fl/fl}$ mice led us to question whether adipose vasculature was also affected by deficiency in myeloid-resident NRP1. Nonbiased transcriptomic analysis by RNA sequencing (RNA-seq) and gene set enrichment analysis (GSEA) of NRP1-deficient peritoneal macrophages revealed a significant decrease in angiogenesis-related genes in knockout macrophages, suggesting that NRP1 contributes to their angiogenic potential (Fig. 3, A and B). To elucidate the role of NRP1$^+$ myeloid cells in adipose vascularization, we investigated blood vessel structure in VAT. Isolectin B4 (lectin) labeling revealed compromised vasculature in LysM-Cre-*Nrp1*$^{fl/fl}$ mice under either HFD or NCD (Fig. 3, C and D), with decreased vessel length and vessel area and increased lacunarity indicative of disorganized vascularization (*27*). These results are consistent with the proangiogenic role of NRP1 mononuclear phagocytes in the CNS (*17*) and in tumors (*16*). Because compromised blood supply can lead to hypoxia, we probed the adipose tissue of control and mice with NRP1-deficient myeloid cells. Significantly more hypoxic zones were detected in LysM-Cre-*Nrp1*$^{fl/fl}$ VAT by pimonidazole adduct staining (Fig. 3E) (*28*). These results suggest that myeloid-resident NRP1 drives adipose tissue vascularization and mitigates hypoxia in obesity.

Macrophage-resident NRP1 mitigates cytokine release and proinflammatory polarization

A heightened inflammatory state is a key feature of hypoxic and hypertrophic adipose tissue. We therefore sought to gain further insight into the role of myeloid-resident NRP1 on ATM polarization. Cell-sorted ATMs isolated from VAT of HFD-fed (Fig. 4A) control and LysM-Cre-*Nrp1*$^{fl/fl}$ mice (Fig. 1A) revealed a significant up-regulation

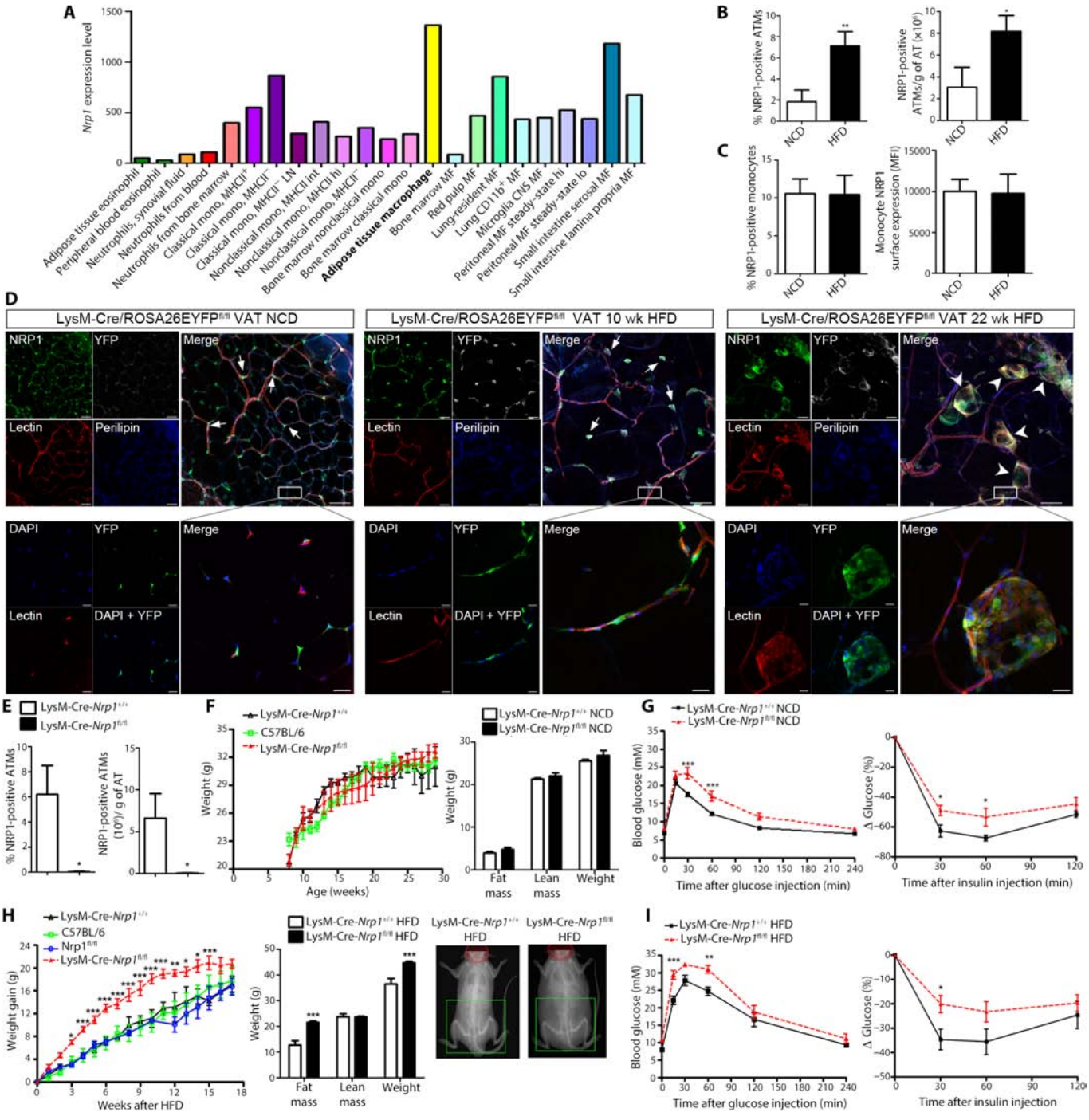

Fig. 1. NRP1-expressing macrophages accumulate in adipose tissue during DIO and regulate weight gain and glucose tolerance. (**A**) *Nrp1* expression levels in populations of eosinophils, neutrophils, monocytes, and macrophages (n = 1 to 4). MHCII, major histocompatibility complex class II; LN, lymph node; MF, macrophage. (**B**) Flow cytometry analysis of NRP1$^+$ ATMs isolated from VAT of WT mice fed either an NCD or a HFD for 10 weeks, represented as percent (left) or total number of cells per gram of tissue (right) (n = 9). (**C**) Flow cytometry analysis of NRP1$^+$ monocytes isolated from WT mice fed either an NCD or a HFD for 4 weeks, represented as percent (left) or MFI (right) (n = 5). (**D**) Representative VAT immunohistochemistry of LysM-Cre/ROSA26EYFP$^{fl/fl}$ mice fed NCD (left), HFD for 10 weeks (middle), and HFD for 22 weeks (right) labeled for NRP1, lectin, and perilipin (magnification, ×30; scale bars, 50 μm; top), and magnification with additional DAPI stain (magnification, ×60; scale bars, 20 μm; bottom). (**E**) Flow cytometry analysis of NRP1$^+$ ATMs isolated from VAT of LysM-Cre-*Nrp1*$^{+/+}$ (control) and LysM-Cre-*Nrp1*$^{fl/fl}$ mice, represented as percent (left) or total number of cells per gram of tissue (right) (n = 6). (**F**) Weight gain of control, LysM-Cre-*Nrp1*$^{fl/fl}$, and WT on NCD for 30 weeks (n = 4 to 9). EchoMRI of control and LysM-Cre-*Nrp1*$^{fl/fl}$ mice 18 weeks on NCD (age-matched controls to HFD mice) (n = 4). (**G**) GTT (n = 12, two experiments) and insulin tolerance test (ITT) (n = 6 to 7, two experiments) of control and LysM-Cre-*Nrp1*$^{fl/fl}$ mice 18 weeks on NCD. (**H**) Weight gain of control, LysM-Cre-*Nrp1*$^{fl/fl}$, *Nrp1*$^{fl/fl}$, and WT on HFD for 18 weeks (n = 4 to 14). EchoMRI and DEXA scan of control and LysM-Cre-*Nrp1*$^{fl/fl}$ mice 10 weeks on HFD (n = 4). (**I**) GTT (n = 9 to 10, two experiments) and ITT (n = 6, two experiments) of control and LysM-Cre-*Nrp1*$^{fl/fl}$ mice 16 weeks on HFD (n = 3). White arrows denote NRP1$^+$ ATMs, and white arrowheads denote NRP1$^+$ CLSs. *P < 0.05, **P < 0.01, ***P < 0.001, Student's unpaired t test (B, C, and E) or two-way ANOVA with Bonferroni post hoc test (F to I).

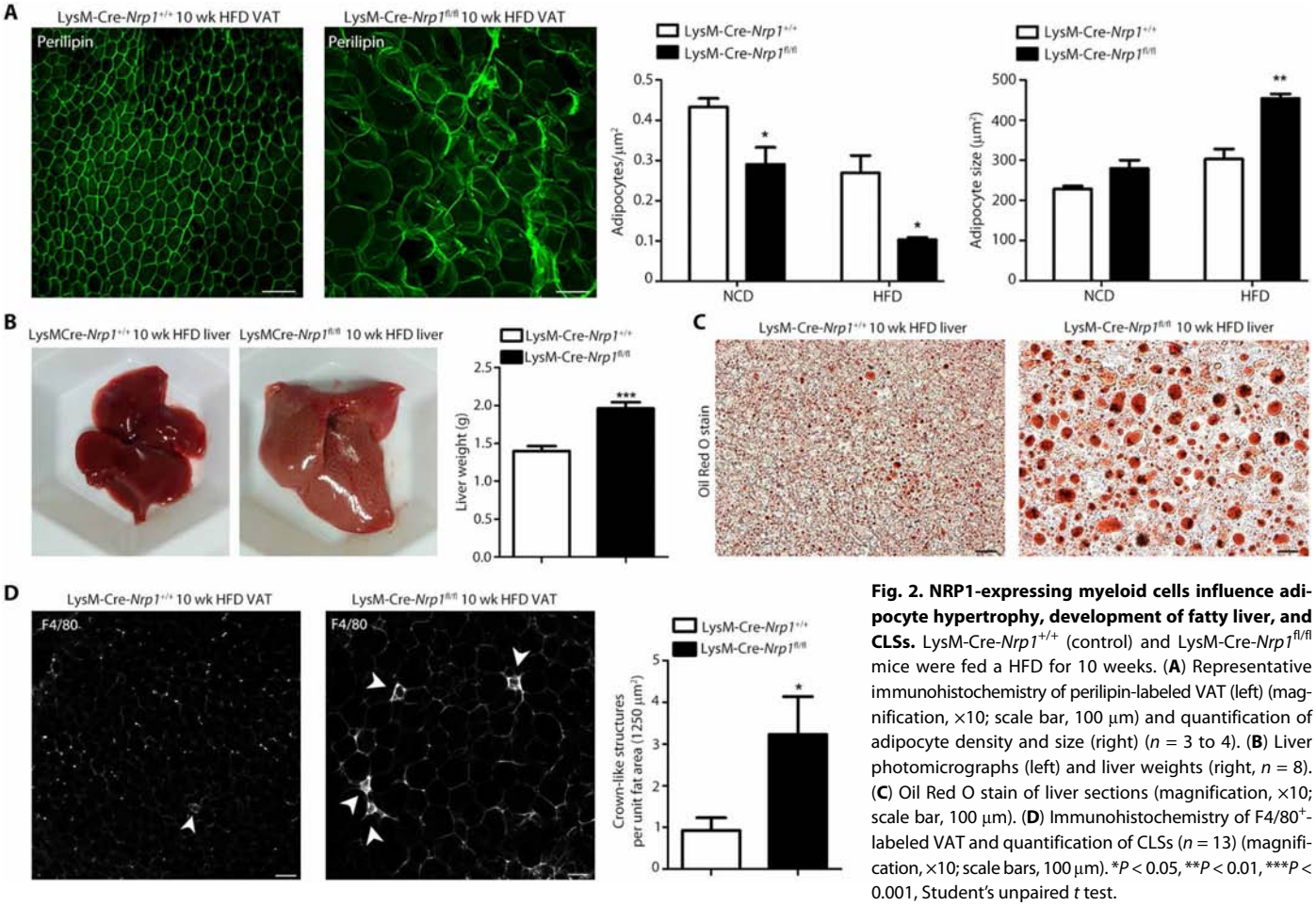

Fig. 2. NRP1-expressing myeloid cells influence adipocyte hypertrophy, development of fatty liver, and CLSs. LysM-Cre-*Nrp1*$^{+/+}$ (control) and LysM-Cre-*Nrp1*$^{fl/fl}$ mice were fed a HFD for 10 weeks. (**A**) Representative immunohistochemistry of perilipin-labeled VAT (left) (magnification, ×10; scale bar, 100 μm) and quantification of adipocyte density and size (right) (n = 3 to 4). (**B**) Liver photomicrographs (left) and liver weights (right, n = 8). (**C**) Oil Red O stain of liver sections (magnification, ×10; scale bar, 100 μm). (**D**) Immunohistochemistry of F4/80$^+$-labeled VAT and quantification of CLSs (n = 13) (magnification, ×10; scale bars, 100 μm). *P < 0.05, **P < 0.01, ***P < 0.001, Student's unpaired t test.

of proinflammatory genes interleukin-6 (*Il-6*), tumor necrosis factor–α (*Tnf-α*), and interleukin-1α (*Il-1α*) (Fig. 4B). GSEA revealed a significant enrichment in Molecular Signatures Database (MSigDB) (*29*) hallmark inflammatory response genes in NRP1-deficient peritoneal macrophages, suggesting that NRP1 mitigates macrophage inflammation (Fig. 4, C and D). These data are consistent with findings that NRP1 expression is associated with an M2 macrophage polarization because its expression is increased in macrophages cultured in conditions that promote M2 activation (*30*).

Within the VAT of HFD-fed LysM-Cre-*Nrp1*$^{fl/fl}$ mice, we detected a significant increase in ATMs (Fig. 4E) and a trend-like increase in neutrophils (Fig. 4F) (see gating scheme, fig. S5A). To determine whether macrophage polarization differed in the absence of NRP1, we quantified expression of the M2 marker CD206 on all ATMs (Fig. 4, G and H) and observed a significant decrease in CD206$^+$ ATMs in LysM-Cre-*Nrp1*$^{fl/fl}$ VAT and a significant increase in proinflammatory CD206$^-$ ATMs (Fig. 4G). In agreement with the proinflammatory M1 phenotype of NRP1-deficient mice, plasma levels of proinflammatory TNF-α, IL-1β, and IFN-γ (interferon-γ) rose in LysM-Cre-*Nrp1*$^{fl/fl}$ mice (Fig. 4I). Together, these data identify a skewed polarization of NRP1-deficient macrophages toward M1 during diet-induced obesity (DIO) that is compounded by heightened accretion of ATMs in LysM-Cre-*Nrp1*$^{fl/fl}$ mice.

Deficiency in myeloid-resident NRP1 affects systemic metabolism

Given the propensity of mice with NRP1-deficient myeloid cells to gain more weight when on HFD, we set out to investigate whether this weight gain was due to increased anabolism or reduction of activity-dependent energy expenditure. We measured food intake and activity (beam breaks) using a telemetry-based monitoring system. We did not observe any difference in total daily food consumption between control and LysM-Cre-*Nrp1*$^{fl/fl}$ mice fed NCD (Fig. 5A). Furthermore, no overall differences in daily activity were detected (Fig. 5B and fig. S2A). LysM-Cre-*Nrp1*$^{fl/fl}$ mice consumed slightly less HFD than control LysM-Cre-*Nrp1*$^{+/+}$ mice (Fig. 2C), indicating that hyperphagia was not driving weight gain. In addition, total activity did not differ significantly, suggesting that the accelerated weight gain of LysM-Cre-*Nrp1*$^{fl/fl}$ mice cannot be attributed to reduced activity either (Fig. 5D and fig. S2B). Metabolic chamber analysis was performed at 9 to 10 weeks after initiation of HFD, a time period where LysM-Cre-*Nrp1*$^{fl/fl}$ had gained significantly more weight than control LysM-Cre-*Nrp1*$^{+/+}$ mice (ranging from 4 to 15 weeks of HFD feeding) (Fig. 1H).

Because accelerated weight gain in LysM-Cre-*Nrp1*$^{fl/fl}$ HFD mice could not be attributed to increased food consumption or decreased activity, we sought to characterize the metabolic phenotype of these mice via indirect calorimetry. After acclimatization, data were collected

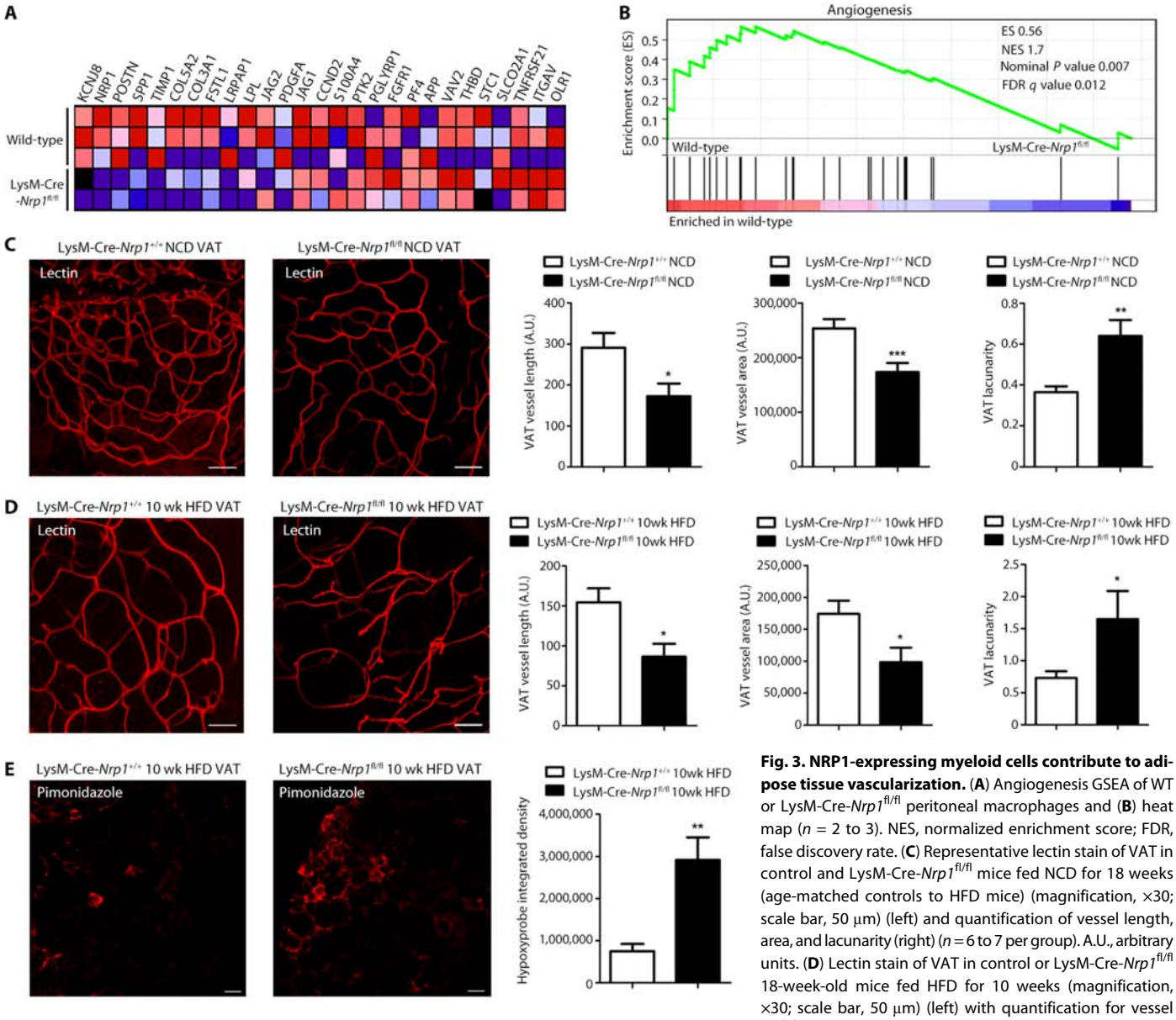

Fig. 3. NRP1-expressing myeloid cells contribute to adipose tissue vascularization. (**A**) Angiogenesis GSEA of WT or LysM-Cre-*Nrp1*$^{fl/fl}$ peritoneal macrophages and (**B**) heat map (n = 2 to 3). NES, normalized enrichment score; FDR, false discovery rate. (**C**) Representative lectin stain of VAT in control and LysM-Cre-*Nrp1*$^{fl/fl}$ mice fed NCD for 18 weeks (age-matched controls to HFD mice) (magnification, ×30; scale bar, 50 μm) (left) and quantification of vessel length, area, and lacunarity (right) (n = 6 to 7 per group). A.U., arbitrary units. (**D**) Lectin stain of VAT in control or LysM-Cre-*Nrp1*$^{fl/fl}$ 18-week-old mice fed HFD for 10 weeks (magnification, ×30; scale bar, 50 μm) (left) with quantification for vessel length, area, and lacunarity (n = 6 to 11 per group). (**E**) Pimonidazole adduct staining of control or LysM-Cre-*Nrp1*$^{fl/fl}$ mice after 10 weeks on HFD (magnification, ×10; scale bar, 100 μm) (left) and quantification of hypoxyprobe stain (right) (n = 7 to 8). *P < 0.05, **P < 0.01, ***P < 0.001, Student's unpaired t test.

and averaged over a 7-day period. LysM-Cre-*Nrp1*$^{fl/fl}$ mice on NCD had similar VO_2 compared with controls, with a slight increase between the transition from light to dark and vice versa (Fig. 5E and fig. S2C). This was mirrored by modestly increased light cycle heat production (Fig. 5F and fig. S2D). Furthermore, the respiratory exchange ratio (RER) of LysM-Cre-*Nrp1*$^{fl/fl}$ mice was also significantly lower in the dark cycle (Fig. 5G and fig. S2E), suggesting a systemic baseline preference for lipids over carbohydrates during periods of activity, likely due to greater availability of FAs in these mice (see below). When fed HFD, LysM-Cre-*Nrp1*$^{fl/fl}$ mice showed considerably lower VO_2 (Fig. 5H and fig. S2F) and heat production (Fig. 5I and fig. S2G), indicative of reduced lipid catabolism in these mice. However, discrepancies in RER observed in NCD were abolished with HFD (Fig. 5J and fig. S2H) because lipids became the predominant combustion source for both mouse strains on HFD. Furthermore, although LysM-Cre-*Nrp1*$^{fl/fl}$ mice maintained similar food intake and activity levels when on HFD, their catabolic rates were significantly reduced, causing accumulation of lipid-based calories.

In addition, levels of plasma low-density lipoprotein (LDL) cholesterol were increased in LysM-Cre-*Nrp1*$^{fl/fl}$ mice after 10 and 22 weeks on HFD (fig. S2I). Similar changes were seen in total cholesterol (fig. S2J). Cholesterol/high-density lipoprotein (HDL) ratios were significantly higher after 22 weeks on HFD (fig. S2K), suggesting that a prolonged HFD exacerbates the metabolic phenotype of LysM-Cre-*Nrp1*$^{fl/fl}$ mice. Together, these data further characterize imbalances in lipid metabolism observed in the LysM-Cre-*Nrp1*$^{fl/fl}$ mice.

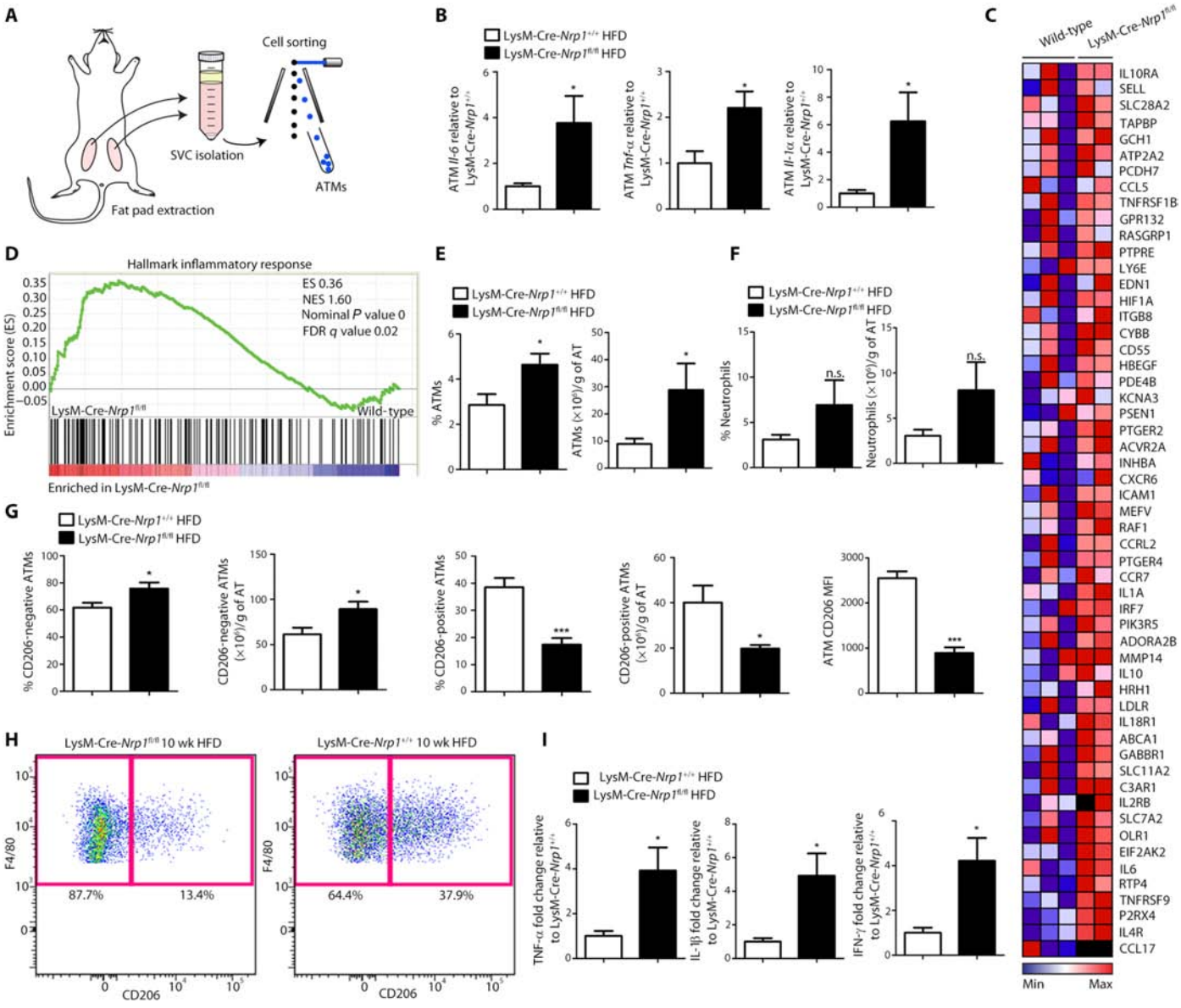

Fig. 4. Macrophage-resident NRP1 mitigates cytokine release and proinflammatory polarization. (**A**) Schematic representation of ATM isolation. SVC, stromal vascular cell. (**B**) qPCRs of *Il-6*, *Tnf-α*, and *Il-1α* in ATMs isolated from 10-week HFD-fed control and LysM-Cre-*Nrp1*$^{fl/fl}$ mice (n = 4 to 7, four experiments). Heat map (**C**) and GSEA (**D**) of inflammatory response genes in WT and LysM-Cre-*Nrp1*$^{fl/fl}$ peritoneal macrophages (n = 2 to 3 per group). (**E** to **H**) Flow cytometry analysis from VAT of LysM-Cre-*Nrp1*$^{+/+}$ (control) or LysM-Cre-*Nrp1*$^{fl/fl}$ mice fed a HFD for 10 weeks representing (E) ATMs in percent (left) or total number of cells per gram of tissue (right) (n = 13 to 17, two experiments). (F) Neutrophils in percent (left) or total number of cells per gram of tissue (right) (n = 6, two experiments). n.s., not significant. (G) CD206$^-$ ATMs in percent or total number of cells per gram of tissue (left), CD206$^+$ ATMs in percent or total number of cells per gram of tissue (middle), or C206 MFI (right) (n = 6, two experiments). (H) FACS dot plot of CD206$^+$ and CD206$^-$ ATMs. (**I**) Plasma TNF-α, IL-1β, and IFN-γ expression of 10-week HFD control and LysM-Cre-*Nrp1*$^{fl/fl}$ mice (n = 5 to 7 per group). *P < 0.05, ***P < 0.001, Student's unpaired t test.

NRP1 regulates lipid uptake in macrophages

FA uptake is a key function of macrophages in adipose tissue, including during clearance of lipid debris from necrotic adipocytes. Given the accumulation of long-chain FAs in obese adipose tissue (*31*, *32*), we assessed the capacity of cell-sorted ATMs from control and LysM-Cre-*Nrp1*$^{fl/fl}$ mice to uptake FAs using a long-chain FA analog (C1-BODIPY-C12; an 18-carbon FA). NRP1-deficient ATMs took up significantly less FAs than control macrophages (Fig. 6A), a finding confirmed in peritoneal macrophages (Fig. 6B). In addition, systemic administration of C1-C12 BODIPY revealed significantly elevated levels of the tagged FAs in VAT and liver of LysM-Cre-*Nrp1*$^{fl/fl}$ mice compared with plasma and heart (Fig. 6C), further substantiating the involvement of NRP1$^+$ macrophages in removing excess lipids in vivo.

To determine whether NRP1 affected lipid uptake in macrophages, we stained for neutral lipids within macrophages with Oil Red O. Oil Red O stain was significantly reduced in LysM-Cre-*Nrp1*$^{fl/fl}$ peritoneal macrophages incubated in adipocyte-conditioned medium (Fig. 6D).

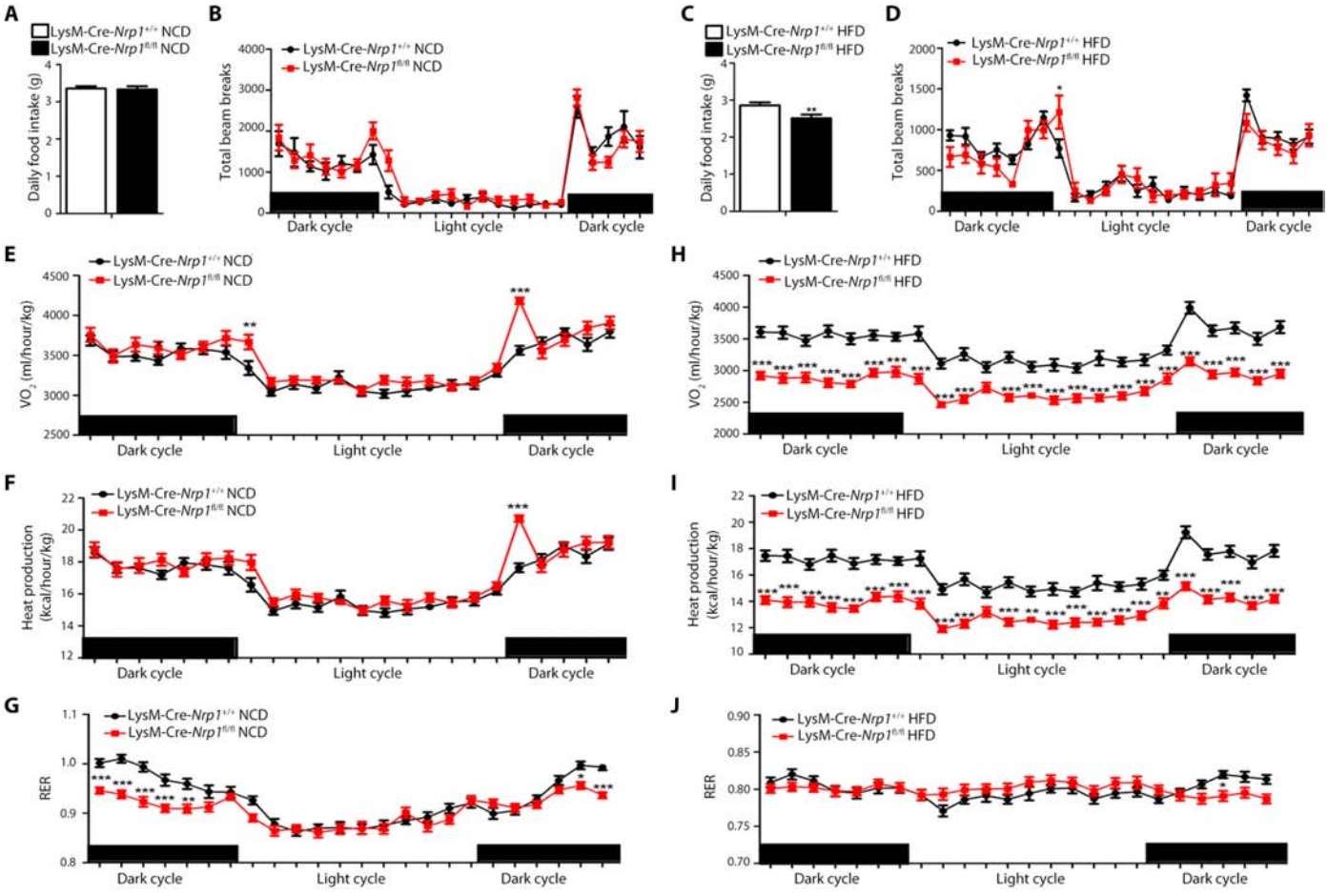

Fig. 5. Deficiency in myeloid-resident NRP1 affects systemic metabolism. Daily food intake (**A**) and total beam breaks (**B**) of control and LysM-Cre-*Nrp1*$^{fl/fl}$ mice after 18 weeks on a regular diet. Daily food intake (**C**) and total beam breaks (**D**) of control and LysM-Cre-*Nrp1*$^{fl/fl}$ of 18-week-old mice after 10 weeks on HFD. VO_2 (**E**), heat production (**F**), and RER (**G**) of control and LysM-Cre-*Nrp1*$^{fl/fl}$ mice 18 weeks on a regular diet. VO_2 (**H**), heat production (**I**), and RER (**J**) of control and LysM-Cre-*Nrp1*$^{fl/fl}$ of 18-week-old mice after 10 weeks on HFD. Data are means ± SEM. *P < 0.05, **P < 0.01, ***P < 0.001, Student's unpaired t test (A and C) and two-way ANOVA with Bonferroni post hoc test (B and D to J) (n = 24, four mice per group). All graph points represent an average calculated over 7 days of measurements.

Because adipocyte and macrophage media differ in glucose and insulin concentration, we assessed whether the decrease in internalized lipids in NRP1-deficient macrophages also occurred in nonconditioned media, including adipocyte medium with and without insulin, as well as macrophage medium. In all conditions, NRP1-deficient macrophages sequestered significantly fewer neutral lipids than controls (fig. S3, A to C).

When assessing the transcriptome of NRP1-deficient macrophages by RNA-seq, the MSigDB hallmark FA metabolism gene set (*33*) revealed that only four genes were differentially regulated when compared with WTs: *Auh*, *Idi1*, *Cpt2*, and *Ehhadh* (Fig. 6E). No significant change was detected in expression levels of the lipid and glucose transporters *Fatp3* or *Glut4* in adipose tissue of HFD-fed LysM-Cre-*Nrp1*$^{fl/fl}$ and control mice (fig. S3, D and E). Furthermore, within the hallmark adipogenesis gene set, which includes the FA uptake facilitator *Cd36*, the FA carrier protein *Fapb4*, and the cholesterol efflux regulatory protein *Abca1*, only *Cpt2* and *Gphn* were up-regulated (Fig. 5F). In addition, no significant changes were detected in lipid digestion, mobilization and transport, or mitochondrial FA β-oxidation gene sets (Fig. 5, G and H). Together, these data suggest that knockdown of *Nrp1* in myeloid cells does not affect the expression levels of the machinery for FA transport, metabolism, or β-oxidation and rather points to a role for NRP1 in lipid uptake.

Deficiency in NRP1 shifts macrophage energy metabolism toward glycolysis

Given the greater adiposity in HFD-fed LysM-Cre-Nrp1$^{fl/fl}$ mice (Fig. 1H) and that FA uptake was impaired in NRP1-deficient macrophages (both ATM and peritoneal), we questioned whether pathways of energy metabolism were differentially engaged in control and NRP1-deficient peritoneal macrophages. We therefore performed functional metabolic analysis specifically assessing rates of glycolysis and FA β-oxidation.

Increased glycolysis was detected in NRP1-deficient macrophages through measurements of the extracellular acidification rate (ECAR) of surrounding media (Fig. 7A). Reliance on enhanced glycolytic metabolism was verified by significantly up-regulated glycolytic acidification, glycolysis, and glycolytic capacity (Fig. 7B), typically detected in classically activated (M1) macrophages (*34*). The significantly reduced basal oxygen consumption rate (OCR)/ECAR ratio detected

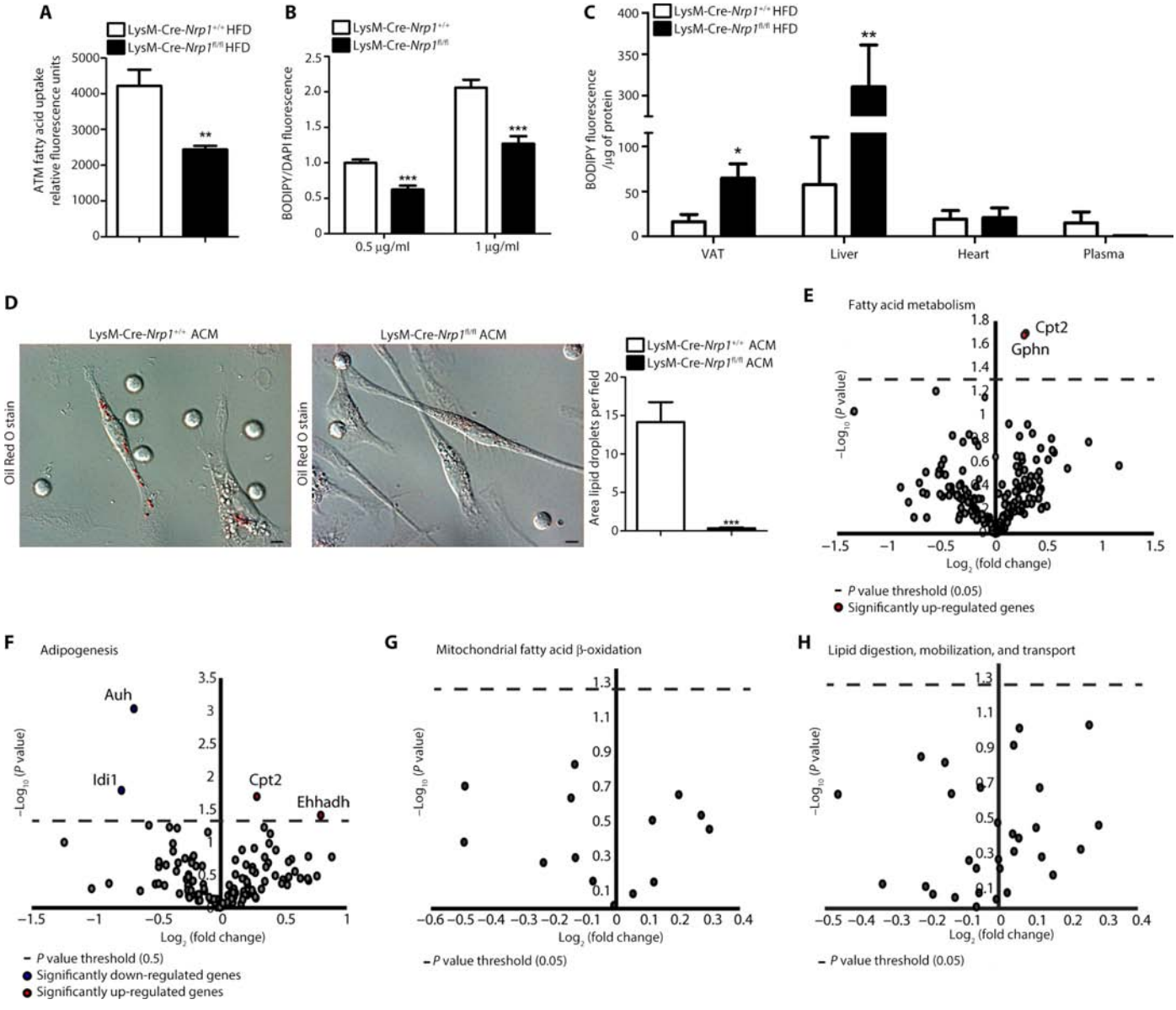

Fig. 6. Macrophage-resident NRP1 promotes FA uptake. (**A**) FA uptake of ATMs isolated from control and LysM-Cre-*Nrp1*$^{fl/fl}$ mice ($n = 4$ to 5, two experiments). (**B**) BODIPY FA analog uptake of peritoneal macrophages isolated from control and LysM-Cre-*Nrp1*$^{fl/fl}$ mice ($n = 7$ to 8, two experiments). (**C**) BODIPY uptake within VAT, liver, plasma, and heart of HFD-fed control and LysM-Cre-*Nrp1*$^{fl/fl}$ mice ($n = 6$ per group). (**D**) Oil Red O stain and quantification of control and LysM-Cre-*Nrp1*$^{fl/fl}$ macrophages incubated in adipocyte-conditioned medium (ACM) (magnification, ×63; scale bars, 10 μm) ($n = 32$ to 35 per group). (**E** to **H**) Volcano plots of changes in RNA-seq expression of peritoneal macrophages from LysM-Cre-*Nrp1*$^{fl/fl}$ compared with WT with (E) MSigDB hallmark gene sets of FA metabolism (M5935), (F) adipogenesis (M5905), (G) mitochondrial FA β-oxidation (M14690), and (H) lipid digestion, mobilization, and transport (M1023). *$P < 0.05$, **$P < 0.01$, ***$P < 0.001$, Student's unpaired *t* test.

in macrophages from LysM-Cre-*Nrp1*$^{fl/fl}$ mice (Fig. 7C) is characteristic of a highly glycolytic metabolism (*35*).

To assess FA oxidation (FAO), we performed baseline OCR measurements on macrophages incubated in bovine serum albumin (BSA) or palmitate. This revealed a small yet significant increase in OCR with palmitate-treated control macrophages (Fig. 7, D and E), but no difference in NRP1-deficient macrophages (Fig. 7E), indicative of low rates of FAO occurring in control but not LysM-Cre-*Nrp1*$^{fl/fl}$ macrophages. A significantly reduced maximal respiratory rate was detected in NRP1-deficient macrophages compared with controls in the presence of both BSA and palmitate (Fig. 7F); however, no significant differences between BSA and palmitate treatments were detected by ECAR (Fig. 7G). Notably, the maximal respiratory rate in the presence of palmitate was significantly lower in LysM-Cre-*Nrp1*$^{fl/fl}$ macrophages compared with BSA. Therefore, exogenous lipids further reduce the mitochondrial efficiency of NRP1-deficient macrophages, indicative of impaired long-chain FA utilization, signifying that an environment found in obese adipose tissue would further compromise energy metabolism within these macrophages. Together, these data suggest that NRP1 participates in FA uptake into the macrophage and allows for β-oxidation, which is associated with less aggressive macrophage polarization. In the absence of NRP1, macrophages favor glycolysis.

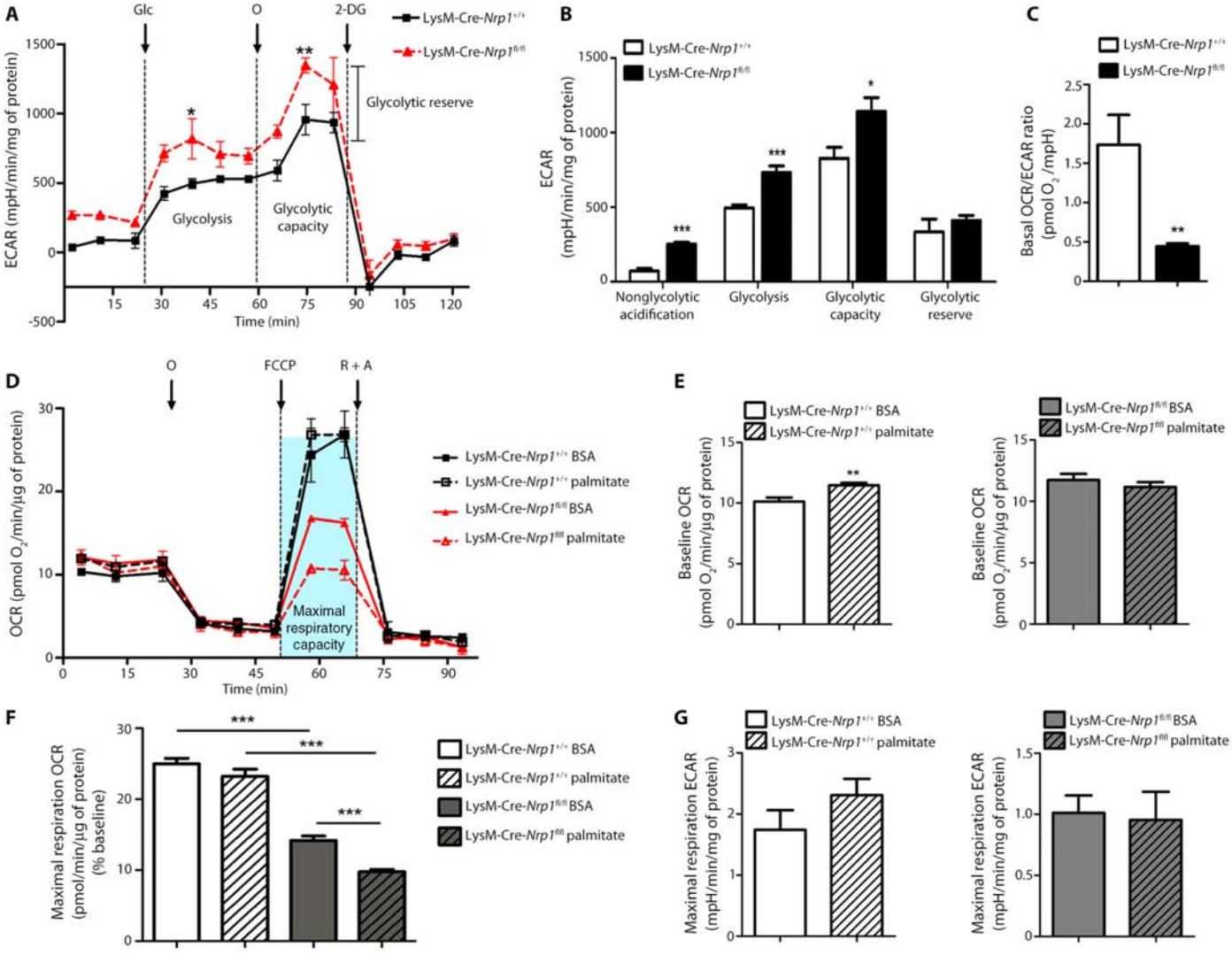

Fig. 7. Deficiency in macrophage-resident NRP1 shifts metabolism to glycolysis. (**A**) ECAR of control and LysM-Cre-*Nrp1*$^{fl/fl}$ macrophages at basal levels, followed by sequential treatment (arrows) of glucose (Glc), oligomycin (O), and 2-DG ($n = 3$, two experiments). (**B**) Nonglycolytic acidification, glycolysis, glycolytic capacity, glycolytic reserve ($n = 3$ to 12) and (**C**) basal OCR/ECAR ratio of control and LysM-Cre-*Nrp1*$^{fl/fl}$ macrophages ($n = 8$ to 9). (**D**) OCR of control and LysM-Cre-*Nrp1*$^{fl/fl}$ macrophages cultured in BSA or palmitate, followed by sequential treatment (arrows) with oligomycin (O), FCCP, and rotenone plus antimycin (R + A) ($n = 2$ to 3, two experiments). Baseline OCR ($n = 6$ to 9) (**E**) and maximal respiration OCR (**F**) of control and LysM-Cre-*Nrp1*$^{fl/fl}$ macrophages treated with BSA or palmitate ($n = 4$ to 6). (**G**) ECAR of BSA- and palmitate-treated control or LysM-Cre-*Nrp1*$^{fl/fl}$ macrophages ($n = 6$). *$P < 0.05$, **$P < 0.01$, ***$P < 0.001$, two-way ANOVA with Bonferroni post hoc test (A), Student's unpaired *t* test (B, C, E, and G), and one-way ANOVA (F).

Transfer of NRP1-expressing hematopoietic cells improves the metabolic phenotype of LysM-Cre-*Nrp1*$^{fl/fl}$ mice

To establish that the effects of NRP1 loss are dependent on loss of NRP1 in the hematopoietic compartment, we next investigated whether bone marrow transfer would restore metabolic health to LysM-Cre-*Nrp1*$^{fl/fl}$ mice. We transferred bone marrow from adult LysM-Cre-*Nrp1*$^{fl/fl}$ mice and LysM-Cre-*Nrp1*$^{+/+}$ control mice to lethally irradiated CD45.1 WT animals (Fig. 8A). Eight weeks after bone marrow transplantation, the circulating population of monocytes expressed donor mouse phenotypes attesting to successful transfer (fig. S5, A and B), and no weight differences among groups were detected (fig. S5, C and D). No significant differences were noted in glucose tolerance of LysM-Cre-*Nrp1*$^{fl/fl}$ recipient mice transplanted with CD45.1 WT bone marrow compared with LysM-Cre-*Nrp1*$^{+/+}$ recipient mice transplanted with CD45.1 WT bone marrow (fig. S5E), indicating that WT bone marrow–derived cells improve glucose tolerance. Furthermore, transplantation with LysM-Cre-*Nrp1*$^{fl/fl}$ bone marrow to CD45.1 recipient mice significantly compromised their glucose tolerance when compared with CD45.1 recipient mice transplanted with LysM-Cre-*Nrp1*$^{+/+}$ bone marrow (fig. S5F). Chimeras were then placed on HFD for 10 weeks, and their VAT was probed for reconstitution differences. Donor mice ATMs and B and T lymphocytes comprised most of the VAT populations probed (Fig. 8B and fig. S5, I to K). Difference in glucose tolerance was further exacerbated after HFD for WT mice reconstituted with LysM-Cre-*Nrp1*$^{fl/fl}$ bone marrow recipients, whereas the glucose tolerance of CD45.1 WT bone marrow

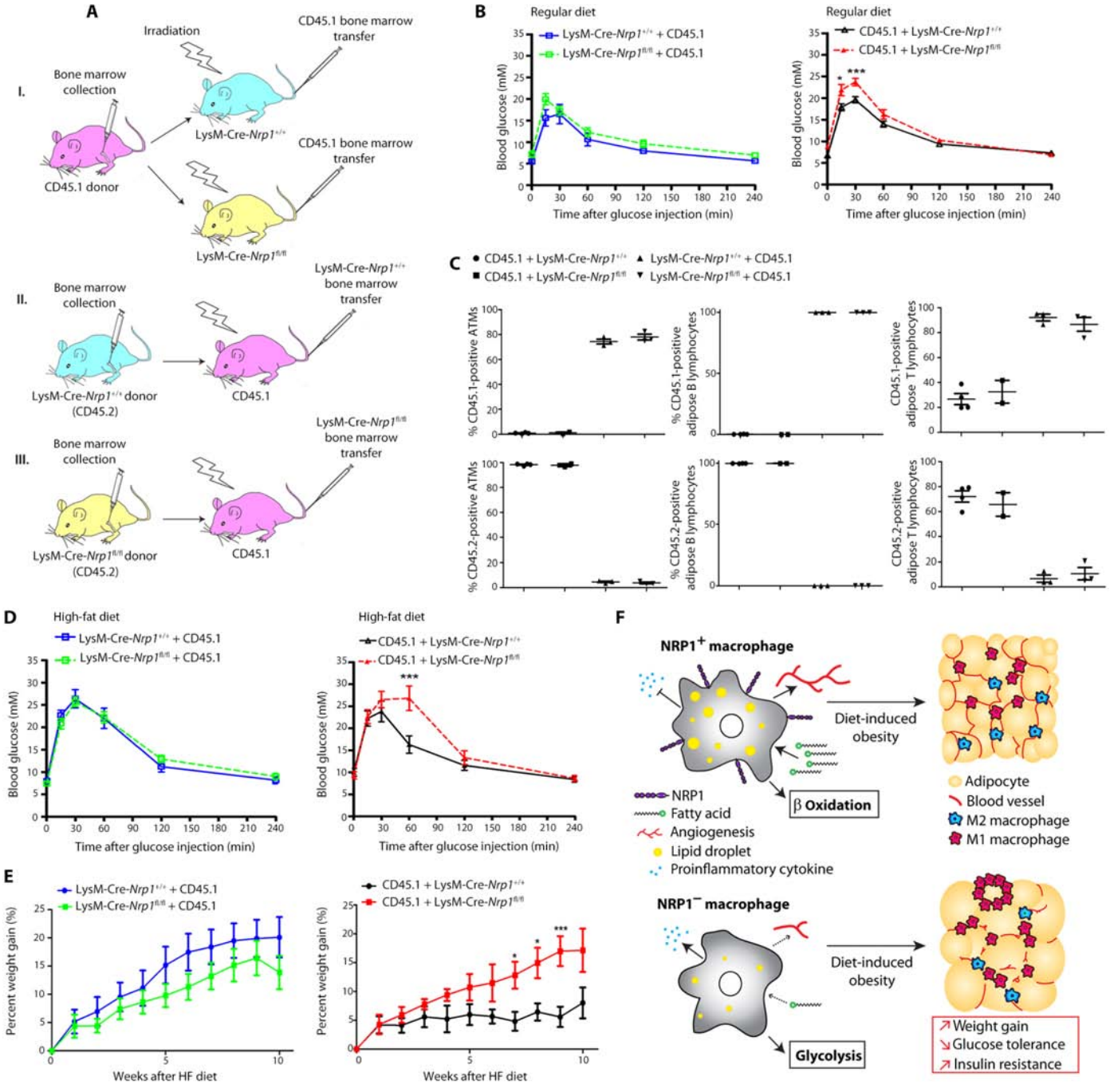

Fig. 8. Transfer of NRP1-expressing bone marrow improves the metabolic phenotype of LysM-Cre-*Nrp1*$^{fl/fl}$ mice. (**A**) Schematic of bone marrow transfer. (**B**) GTT of bone marrow chimeras before HFD feeding: LysM-Cre-*Nrp1*$^{+/+}$ or LysM-Cre-*Nrp1*$^{fl/fl}$ plus CD45.1 bone marrow (left; $n = 4$ to 7 per group, two experiments), and CD45.1 plus LysM-Cre-*Nrp1*$^{+/+}$ or LysM-Cre-*Nrp1*$^{fl/fl}$ bone marrow (right; $n = 6$ to 7, two experiments). (**C**) Flow cytometry analysis showing reconstitution of CD45.1$^+$ and CD45.2$^+$ ATMs and B and T lymphocytes isolated from chimera VAT ($n = 2$ to 4). (**D**) GTT of LysM-Cre-*Nrp1*$^{+/+}$ or LysM-Cre-*Nrp1*$^{fl/fl}$ mice plus CD45.1 bone marrow (left; $n = 6$ to 7 per group, two experiments) and GTT of CD45.1 mice plus LysM-Cre-*Nrp1*$^{+/+}$ or LysM-Cre-*Nrp1*$^{fl/fl}$ bone marrow (right; $n = 5$ to 7 per group) on HFD. (**E**) Percent weight gain when on HFD of LysM-Cre-*Nrp1*$^{+/+}$ or LysM-Cre-*Nrp1*$^{fl/fl}$ mice plus CD45.1 bone marrow (left; $n = 8$ per group) and percent weight gain of CD45.1 mice plus LysM-Cre-*Nrp1*$^{+/+}$ or LysM-Cre-*Nrp1*$^{fl/fl}$ bone marrow (right; $n = 5$ to 7 per group). (**F**) Recapitulative schematic of NRP1$^+$ and NRP1$^-$ ATMs in adipose tissue homeostasis. $^*P < 0.05$, $^{***}P < 0.001$, two-way ANOVA with Bonferroni post hoc test (C and D).

recipients did not differ (Fig. 8C and fig. S5, G and H). In addition, whereas recipients of control LysM-Cre-*Nrp1*$^{+/+}$ bone marrow did not differ in weight gain upon HFD, recipients of LysM-Cre-*Nrp1*$^{fl/fl}$ bone marrow gained significantly more weight (Fig. 8D). These results demonstrate that the LysM-Cre-*Nrp1*$^{fl/fl}$ phenotype is dependent on loss of NRP1 in the hematopoietic compartment. In addition to

confirming the importance of NRP1$^+$ myeloid cells in weight gain and glucose tolerance, these results also suggest that circulating monocytes contribute to glucose intolerance and weight gain (Fig. 8E).

DISCUSSION

The present study identifies a subset of ATMs that accumulate in adipose tissue and promote healthy adipose expansion while safeguarding against metabolic complications ensuing from elevated caloric intake. More precisely, we demonstrate a critical role for NRP1 in driving FA uptake in ATMs and hence substrate availability for consumption in β-oxidation that typically fuels a reparative and homeostatic M2 phenotype. Inefficient at burning FAs, NRP1-deficient macrophages revert to a characteristic aggressive glycolysis-reliant M1-like phenotype and contribute to tissue dysfunction, glucose intolerance, and insulin insensitivity. Therefore, in the absence of myeloid-resident NRP1, FAs are not efficiently catabolized by macrophages, contributing to rapid weight gain. Our findings also support the notion that adipose tissue plasticity is critical for healthy weight gain and implicate NRP1$^+$ ATMs in the process. In this regard, lack of NRP1 on ATMs perturbs adipose vasculature, leading to hypoxic zones in VAT and compromised glucose tolerance both during normal development and in DIO. Bone marrow transfer of NRP1$^+$ cells improves glucose homeostasis, suggesting that weight gain and glucose tolerance can be significantly modulated through transferred hematopoietic cells.

Although a local proinflammatory response in adipocytes has been suggested to be an adaptive measure to enable safe storage of excess nutrients (*8*), our study provides evidence that hematopoietic expression of NRP1 is sufficient to influence adipose tissue expansion and affect overall metabolic health. Our data also highlight the importance of adequate matching of adipose vascular supply through proportional, concomitant vascularization during development as well as during adult fat pad expansion. Adipose tissue angiogenesis has been proposed to be essential for fat pad expansion and therefore a potential process to target therapeutically for morbid weight gain, much as had been proposed for tumor growth (*36*–*41*). Yet, adipose neovascularization also provides adequate oxygen and trophic support, FA exchange, and evacuation lines for metabolic waste products. When adipocyte hypertrophy outpaces blood vessel growth, hypoxic zones form, influencing macrophage polarization and exacerbating inflammation (*42*–*45*). Hence, vascular rarefication or antiangiogenic strategies in expanding adipose tissue may contribute to metabolic complications associated with obesity. Therefore, our data support the importance of adipose vascular plasticity during adult fat pad expansion.

Here, we specifically interrogated on the role of myeloid-resident NRP1, yet NRP1 is also expressed by murine brown adipocytes (*46*) and bone marrow adipocytes (*47*), where it inhibits hematopoiesis (*48*). Hence, it will be interesting to assess the local contribution of NRP1 in these tissues to overall adipose dynamics. Notably, although our findings on ATM-resident NRP1 were corroborated in vitro, the LysM (or Lys2) promoter used in our study to express Cre in macrophages in vivo is also expressed in neutrophils and, to an extent, in a subset of T and B cells (*49*). Neutrophils express high levels of LysM, and therefore, we cannot fully discount their contribution to the phenotype observed. However, ATMs express significantly more *Nrp1* than neutrophils, and the macrophage population remains most affected by the targeted deletion. Future work elucidating the mechanisms by which NRP1 promotes FA uptake and β-oxidation will be required. Insight gained may be important toward designing therapeutic modalities for metabolic syndromes.

Overall, our work identifies NRP1$^+$ ATMs as promoters of healthy weight gain and describes a myeloid-based mechanism for glucose intolerance even independent of excessive weight gain because type 2 diabetes mellitus can occur in individuals with a normal body mass index (*50*). Our study further provides in vivo support for the notion that macrophage polarization is intrinsically associated with energy metabolism and that homeostatic macrophages rely heavily upon FAs delivered via NRP1, a slower yet sustained means of energy production. More broadly, our study provides insight into the essential role of macrophages in adipose tissue homeostasis.

MATERIALS AND METHODS

Mice

All studies were performed according to the guidelines of the Canadian Council on Animal Care and were approved by the Animal Care Committee of the Maisonneuve-Rosemont Hospital Research Center. C57BL/6 WT mice, strain appropriate LysM-Cre mice controls [B6.129P2-*Lyz2*$^{tm1(cre)Ifo}$/J; #004781], NRP1 floxed mice [B6.129(SJL)-*Nrp1*^{tm2Ddg}/J; #005247], and B6SJL mice (B6.SJL-*Ptprc*^{a} *Pepc*^{b}/BoyJ; #002014) were purchased from the Jackson Laboratory and bred in house. Mice were fed either NCD (18% kcal fat, 2018 Teklad Global) or HFD (59% kcal fat, BioServ F3282) starting at 8 weeks of age for 10 to 32 weeks. See Supplementary Experimental Procedures for full details on study design.

Bone marrow chimeras

For the generation of chimeric mice, bone marrow cells were obtained by flushing both tibias, femurs, and iliac crests of 8-week-old WT B6.SJL (CD45.1), LysM-Cre-*Nrp1*$^{+/+}$ (CD45.2), or LysM-Cre-*Nrp1*$^{fl/fl}$ (CD45.2) donor mice. Eight-week-old B6.SJL, LysM-Cre-*Nrp1*$^{+/+}$, or LysM-Cre-*Nrp1*$^{fl/fl}$ recipient mice were lethally irradiated (12 Gy) and reconstituted with 5×10^6 bone marrow cells. Glucose tolerance tests (GTTs) were performed on chimeric mice 8 weeks after reconstitution and then put on HFD for 10 weeks.

Metabolic chamber analysis

Mice were acclimatized to metabolic cages for 7 days, and data were collected over 7 subsequent days. LabMaster/PhenoMaster system from TSE Systems (Germany) measured indirect calorimetry, O_2 consumption and CO_2 production, RER, energy expenditure, food and water intake, and locomotor activity by infrared beam breaking. Mice were placed in metabolic chambers for a 1-week acclimatization period, followed by 1 week of data collection.

ImmGen skyline data set

ImmGen data phase 1 [Gene Expression Omnibus (GEO) accession code GSE15907] and phase 2 (GSE37448) were extracted and normalized in R by Robust Multi-array Average (RMA), and antilog values were plotted.

Glucose tolerance test

Mice were starved for 12 hours overnight. Blood glucose was measured (Accu-Chek, Roche) at baseline and at 15, 30, 60, 120, and 240 min after intraperitoneal injection of 10% D-glucose (2 mg/kg; Sigma).

Insulin tolerance test

Mice were starved for 5.5 hours (in the morning). Blood glucose was measured at baseline and at 30, 60, and 120 min after intraperitoneal injection of insulin (0.75 U/kg; Novo Nordisk).

FACS of ATMs

White adipose tissue was collected, weighted, and homogenized in Dulbecco's modified Eagle's medium (DMEM)/F12 medium and then incubated with collagenase D (1 mg/ml; Sigma) at 37°C for 45 min. EDTA was then added at a concentration of 10 mM, and the mix was incubated for an extra 5 min. Homogenates were then filtered with a 70-μm cell strainer and centrifuged. Pellets were resuspended and incubated in lysis buffer (10 mM $KCHO_3$, 150 mM NH_4Cl, 0.1 mM EDTA) for 5 min at room temperature and centrifuged. Pellets were resuspended in 1× phosphate-buffered saline (PBS) and filtered with a 100-μm cell strainer. Cell suspensions were incubated with the Zombie Aqua Fixable Viability Kit (BioLegend) for 15 min at room temperature. Cells were then incubated with LEAF purified anti-mouse CD16/32 (BioLegend) for 15 min at room temperature to block Fc receptors. Cells were then incubated for 25 min at 4°C, with antibodies listed in table S1. For analysis of CD206 expression, permeabilization and fixation of the cells were done using the Cytofix/Cytoperm Kit (BD Biosciences) at 4°C for 20 min. Cells were then incubated with rat serum (Cedarlane) for 25 min at 4°C to block intracellular receptors. Cells were then stained with Brilliant Violet 421 anti-mouse CD206 (MMR) (BioLegend) for 25 min at 4°C. FACS was performed on a Fortessa (BD Biosciences) device, and data were analyzed using FlowJo software (version 7.6.5).

ATM FA uptake

The fluorometric Free Fatty Acid Uptake Assay Kit (Abcam) was used to detect ATM FA uptake. Cell-sorted ATMs were isolated from VAT of HFD-fed LysM-Cre-*Nrp1*$^{+/+}$ or LysM-Cre-*Nrp1*$^{fl/fl}$ mice and plated at a density of 100,000 cells per well in a 96-well plate. After overnight incubation in complete DMEM/F12 medium, ATMs were serum-deprived for 1 hour in 100-μl basal medium. FA dye loading solution (100 μl) was added to each well (including blanks) and incubated for 30 min. Fluorescence intensity was measured at an excitation wavelength of 485 and at an emission wavelength of 515 nm.

Glycolysis and FAO assays

Real-time analysis ECAR and OCR were performed on LysM-Cre-*Nrp1*$^{+/+}$ and LysM-Cre-*Nrp1*$^{fl/fl}$ peritoneal macrophages with the XF-24 Extracellular Flux Analyzer (Seahorse Bioscience). For glycolysis assays, macrophages were cultured in a 24-well Seahorse plate at a seeding density of 1.75×10^5 cells per well. Before experiment, medium was changed to Seahorse DMEM containing 2 mM glutamine and 0.5% BSA. Glucose (10 mM; Sigma), oligomycin (1.5 μM; Sigma), and 2-deoxy-D-glucose (2-DG) (50 mM; Sigma) were sequentially added. For FAO assays, macrophages were cultured in a 24-well Seahorse plate at a seeding density of 2×10^5 cells per well. Before experiment, medium was changed to Seahorse DMEM containing 10 mM glucose, 2 mM glutamine, 1 mM pyruvate, 1 mM carnitine, and 0.5% BSA (BSA group). Selected wells received an additional 0.3 mM palmitate (palmitate-BSA group; Sigma). Oligomycin (1.5 μM; Sigma), carbonyl cyanide *p*-trifluoromethoxyphenylhydrazone (FCCP) (5 μM), 1 μM rotenone, and 2 μM antimycin A were sequentially added. Upon completion of glycolysis and FAO experiments, cells were lysed and their protein content was quantified. OCR and ECAR data were normalized to protein content.

Quantitative real time polymerase chain reaction analysis

RNA extraction was performed with 100 to 500 mg of frozen (−80°C) VAT after the TRIzol Reagent Protocol (Invitrogen). Total RNA (1 μg) was reverse-transcribed according to the manufacturer's instructions (iScript cDNA Synthesis Kit, Bio-Rad). Quantitative polymerase chain reaction (qPCR) was performed using SYBR Green (Bio-Rad) and 40 ng of complementary DNA (cDNA) per reaction (7500 Real-Time PCR System, Applied Biosystems). Expression levels were normalized to the expression of β-actin. Primer (Integrated DNA Technologies) sequences are listed in table S2.

Vascular analysis

AngioTool analysis (*27*) was performed on 10× epifluorescent photomicrographs of lectin-stained VAT.

Immunohistochemistry

VAT tissue was fixed in 4% paraformaldehyde (PFA) (Electron Microscopy Sciences) for 48 hours and then incubated in 20% methanol (Chaptec) for 10 min and rinsed in PBS. One-hour blocking in 3% BSA (HyClone, GE) plus 0.3% Triton X-100 (Sigma) preceded overnight incubation with rhodamine-labeled Griffonia (Bandeiraea) Simplicifolia Lectin I (Vector Laboratories Inc.), anti-rat F4/80 [donkey immunoglobulin G (IgG), eBioscience], anti-rabbit perilipin (donkey IgG, Abcam), and anti-rat NRP1 antibody (donkey IgG, R&D Systems) at 4°C. Alexa Fluor secondary antibodies were incubated for 2 hours at 20°C. The VAT was then mounted onto a microscope slide, and images were taken by confocal microscope.

In vivo hypoxyprobe detection

Hypoxyprobe injections were performed on LysM-Cre-*Nrp1*$^{+/+}$ and LysM-Cre-*Nrp1*$^{fl/fl}$ male mice fed with HFD for 10 weeks or age-matched NCD. Pimonidazole (60 mg/kg; Hypoxyprobe-Red549, Hypoxyprobe) diluted in 0.9% saline (Hospira) was injected intraperitoneally. Mice were euthanized 1 hour after hypoxyprobe injection. VAT samples were collected and fixed in 4% PFA (Electron Microscopy Sciences) for pimonidazole adduct immunohistochemistry.

RNA-seq sample preparation and sequencing

Total RNA was isolated from macrophages using the RNeasy Mini Kit (Qiagen). The mRNA was then purified from 1 μg of total RNA using the Dynabeads mRNA DIRECT Micro Kit (Thermo Fisher Scientific). Whole-transcriptome libraries were prepared using the Ion Total RNA-seq Kit v2. The yield and size distribution of the amplified libraries were assessed with the Agilent Bioanalyzer using the DNA 1000 Kit. Sequencing was performed on an Ion Chef instrument (Ion Torrent, Thermo Fisher Scientific).

cDNA library construction and sequencing

Analysis was performed using the Torrent Suite software v4.4 (Thermo Fisher Scientific) and the whole Transcriptome Analysis Plugin version 4.2-r7 (Thermo Fisher Scientific). The whole Transcriptome Analysis Plugin aligns reads on mouse reference genome (mm10) using TopHat2, and then unmapped reads are aligned using Bowtie2 and merged together. FPKM (fragment per kilobase of transcript per million) is calculated using Cufflinks.

Gene set enrichment analysis

GSEA was conducted using GSEA v2.2.1 software provided by Broad Institute of Massachusetts Institute of Technology and Harvard University. We used GSEA to validate correlation between molecular signatures in phenotypes of interest. Enrichment analysis was conducted with $\log_2$-normalized FPKM data generated by the TopHat/Cuffdiff command pipeline: FPKM values were converted as ratios ($FPKM_x$/[$FPKM_{Control}$] mean) and then $\log_2$-normalized ($\log_2$[ratio]) and median-centered ($\log_2$ ratio − [$\log_2$ $ratio_{Control}$] mean). Default parameters were changed as follows: Gene sets of interest were found in a catalog of functional annotated gene sets from MSigDB; phenotype was permutated 1000 times; phenotype label was defined as "Nrp1 knockout" versus "Control"; gene sets smaller than 15 and larger than 500 were excluded from the analysis; statistic used to score hits was defined as "weighted p2," and the class separation metric used was "*t* test."

Statistical analyses

We used an unpaired two-tailed Student's *t* test and one-way or two-way analysis of variance (ANOVA) with Bonferroni post hoc analysis, where appropriate, to compare the different groups. $P < 0.05$ was considered statistically different, denoted graphically as $^*P < 0.05$, $^{**}P < 0.01$, and $^{***}P < 0.001$. Data are means ± SEM. Biological experiment numbers were listed in figure legends.

Primary macrophage culture

See Supplementary Experimental Procedures.

Macrophage BODIPY intake

See Supplementary Experimental Procedures.

In vivo BODIPY uptake

See Supplementary Experimental Procedures.

In vitro differentiation of L1-3T3 adipocytes

See Supplementary Experimental Procedures.

Oil Red O staining and quantification

See Supplementary Experimental Procedures.

Bio-Plex analysis

See Supplementary Experimental Procedures.

SUPPLEMENTARY MATERIALS

immunology.sciencemag.org/cgi/content/full/3/21/eaan4626/DC1
Experimental Procedures
Fig. S1. NRP1-expressing ATMs accumulate in DIO.
Fig. S2. Deficiency in myeloid-resident NRP1 influences systemic metabolism.
Fig. S3. Macrophage-resident NRP1 promotes FA uptake.
Fig. S4. Gating scheme for ATMs.
Fig. S5. Transfer of NRP1-expressing bone marrow.
Table S1. Fluorophore-conjugated antibodies used for flow cytometry.
Table S2. Primer sets used for reverse transcription PCR.
Table S3. Raw data.

REFERENCES AND NOTES

1. G. Taubes, Insulin resistance. Prosperity's plague. *Science* **325**, 256–260 (2009).
2. S. P. Weisberg, D. McCann, M. Desai, M. Rosenbaum, R. L. Leibel, A. W. Ferrante Jr., Obesity is associated with macrophage accumulation in adipose tissue. *J. Clin. Invest.* **112**, 1796–1808 (2003).
3. H. Kanda, S. Tateya, Y. Tamori, K. Kotani, K.-i. Hiasa, R. Kitazawa, S. Kitazawa, H. Miyachi, S. Maeda, K. Egashira, M. Kasuga, MCP-1 contributes to macrophage infiltration into adipose tissue, insulin resistance, and hepatic steatosis in obesity. *J. Clin. Invest.* **116**, 1494–1505 (2006).
4. J. M. Olefsky, C. K. Glass, Macrophages, inflammation, and insulin resistance. *Annu. Rev. Physiol.* **72**, 219–246 (2010).
5. S. U. Amano, J. L. Cohen, P. Vangala, M. Tencerova, S. M. Nicoloro, J. C. Yawe, Y. Shen, M. P. Czech, M. Aouadi, Local proliferation of macrophages contributes to obesity-associated adipose tissue inflammation. *Cell Metab.* **19**, 162–171 (2014).
6. O. Osborn, J. M. Olefsky, The cellular and signaling networks linking the immune system and metabolism in disease. *Nat. Med.* **18**, 363–374 (2012).
7. X. Xu, A. Grijalva, A. Skowronski, M. van Eijk, M. J. Serlie, A. W. Ferrante Jr., Obesity activates a program of lysosomal-dependent lipid metabolism in adipose tissue macrophages independently of classic activation. *Cell Metab.* **18**, 816–830 (2013).
8. I. Wernstedt Asterholm, C. Tao, T. S. Morley, Q. A. Wang, F. Delgado-Lopez, Z. V. Wang, P. E. Scherer, Adipocyte inflammation is essential for healthy adipose tissue expansion and remodeling. *Cell Metab.* **20**, 103–118 (2014).
9. C. Pang, Z. Gao, J. Yin, J. Zhang, W. Jia, J. Ye, Macrophage infiltration into adipose tissue may promote angiogenesis for adipose tissue remodeling in obesity. *Am. J. Physiol. Endocrinol. Metab.* **295**, E313–E322 (2008).
10. C.-H. Cho, Y. J. Koh, J. Han, H.-K. Sung, H. Jong Lee, T. Morisada, R. A. Schwendener, R. A. Brekken, G. Kang, Y. Oike, T.-S. Choi, T. Suda, O.-J. Yoo, G. Y. Koh, Angiogenic role of LYVE-1–positive macrophages in adipose tissue. *Circ. Res.* **100**, e47–e57 (2007).
11. K. B. Cullberg, T. Christiansen, S. K. Paulsen, J. M. Bruun, S. B. Pedersen, B. Richelsen, Effect of weight loss and exercise on angiogenic factors in the circulation and in adipose tissue in obese subjects. *Obesity* **21**, 454–460 (2013).
12. C. E. Hagberg, A. Falkevall, X. Wang, E. Larsson, J. Huusko, I. Nilsson, L. A. van Meeteren, E. Samen, L. Lu, M. Vanwildemeersch, J. Klar, G. Genove, K. Pietras, S. Stone-Elander, L. Claesson-Welsh, S. Ylä-Herttuala, P. Lindahl, U. Eriksson, Vascular endothelial growth factor B controls endothelial fatty acid uptake. *Nature* **464**, 917–921 (2010).
13. C. Raimondi, J. T. Brash, A. Fantin, C. Ruhrberg, NRP1 function and targeting in neurovascular development and eye disease. *Prog. Retin. Eye Res.* **52**, 64–83 (2016).
14. E. Geretti, A. Shimizu, M. Klagsbrun, Neuropilin structure governs VEGF and semaphorin binding and regulates angiogenesis. *Angiogenesis* **11**, 31–39 (2008).
15. C. A. Staton, I. Kumar, M. W. R. Reed, N. J. Brown, Neuropilins in physiological and pathological angiogenesis. *J. Pathol.* **212**, 237–248 (2007).
16. A. Casazza, D. Laoui, M. Wenes, S. Rizzolio, N. Bassani, M. Mambretti, S. Deschoemaeker, J. A. Van Ginderachter, L. Tamagnone, M. Mazzone, Impeding macrophage entry into hypoxic tumor areas by Sema3A/Nrp1 signaling blockade inhibits angiogenesis and restores antitumor immunity. *Cancer Cell* **24**, 695–709 (2013).
17. A. Dejda, G. Mawambo, A. Cerani, K. Miloudi, Z. Shao, J.-F. Daudelin, S. Boulet, M. Oubaha, F. Beaudoin, N. Akla, S. Henriques, C. Menard, A. Stahl, J.-S. Delisle, F. A. Rezende, N. Labrecque, P. Sapieha, Neuropilin-1 mediates myeloid cell chemoattraction and influences retinal neuroimmune crosstalk. *J. Clin. Invest.* **124**, 4807–4822 (2014).
18. T. S. P. Heng, M. W. Painter; Immunological Genome Project Consortium, The Immunological Genome Project: Networks of gene expression in immune cells. *Nat. Immunol.* **9**, 1091–1094 (2008).
19. B. Chaudhary, Y. S. Khaled, B. J. Ammori, E. Elkord, Neuropilin 1: Function and therapeutic potential in cancer. *Cancer Immunol. Immunother.* **63**, 81–99 (2014).
20. T. Kawasaki, T. Kitsukawa, Y. Bekku, Y. Matsuda, M. Sanbo, T. Yagi, H. Fujisawa, A requirement for neuropilin-1 in embryonic vessel formation. *Development* **126**, 4895–4902 (1999).
21. Z. He, M. Tessier-Lavigne, Neuropilin is a receptor for the axonal chemorepellent Semaphorin III. *Cell* **90**, 739–751 (1997).
22. A. Dejda, G. Mawambo, J.-F. Daudelin, K. Miloudi, N. Akla, C. Patel, E. M. M. A. Andriessen, N. Labrecque, F. Sennlaub, P. Sapieha, Neuropilin-1–expressing microglia are associated with nascent retinal vasculature yet dispensable for developmental angiogenesis. *Invest. Ophthalmol. Vis. Sci.* **57**, 1530–1536 (2016).
23. S. Cinti, G. Mitchell, G. Barbatelli, I. Murano, E. Ceresi, E. Faloia, S. Wang, M. Fortier, A. S. Greenberg, M. S. Obin, Adipocyte death defines macrophage localization and function in adipose tissue of obese mice and humans. *J. Lipid Res.* **46**, 2347–2355 (2005).
24. J. J. Berger, R. J. Barnard, Effect of diet on fat cell size and hormone-sensitive lipase activity. *J. Appl. Physiol.* **87**, 227–232 (1999).
25. S. Wueest, R. A. Rapold, J. M. Rytka, E. J. Schoenle, D. Konrad, Basal lipolysis, not the degree of insulin resistance, differentiates large from small isolated adipocytes in high-fat fed mice. *Diabetologia* **52**, 541–546 (2009).
26. S. Nielsen, Z. Guo, C. M. Johnson, D. D. Hensrud, M. D. Jensen, Splanchnic lipolysis in human obesity. *J. Clin. Invest.* **113**, 1582–1588 (2004).
27. E. Zudaire, L. Gambardella, C. Kurcz, S. Vermeren, A computational tool for quantitative analysis of vascular networks. *PLOS ONE* **6**, e27385 (2011).

28. G. E. Arteel, R. G. Thurman, J. A. Raleigh, Reductive metabolism of the hypoxia marker pimonidazole is regulated by oxygen tension independent of the pyridine nucleotide redox state. *Eur. J. Biochem.* **253**, 743–750 (1998).
29. A. Liberzon, A. Subramanian, R. Pinchback, H. Thorvaldsdóttir, P. Tamayo, J. Mesirov, Molecular signatures database (MSigDB) 3.0. *Bioinformatics* **27**, 1739–1740 (2011).
30. J.-D. Ji, K.-H. Park-Min, L. B. Ivashkiv, Expression and function of semaphorin 3A and its receptors in human monocyte-derived macrophages. *Hum. Immunol.* **70**, 211–217 (2009).
31. P. D. Berk, S.-L. Zhou, C.-L. Kiang, D. D. Stump, X. Fan, M. W. Bradbury, Selective up-regulation of fatty acid uptake by adipocytes characterizes both genetic and diet-induced obesity in rodents. *J. Biol. Chem.* **274**, 28626–28631 (1999).
32. O. Petrescu, X. Fan, P. Gentileschi, S. Hossain, M. Bradbury, M. Gagner, P. D. Berk, Long-chain fatty acid uptake is upregulated in omental adipocytes from patients undergoing bariatric surgery for obesity. *Int. J. Obes.* **29**, 196–203 (2005).
33. A. Liberzon, C. Birger, H. Thorvaldsdóttir, M. Ghandi, J. P. Mesirov, P. Tamayo, The Molecular Signatures Database (MSigDB) hallmark gene set collection. *Cell Syst.* **1**, 417–425 (2015).
34. J.-C. Rodríguez-Prados, P. G. Través, J. Cuenca, D. Rico, J. Aragonés, P. Martín-Sanz, M. Cascante, L. Boscá, Substrate fate in activated macrophages: A comparison between innate, classic, and alternative activation. *J. Immunol.* **185**, 605–614 (2010).
35. P. A. Kramer, S. Ravi, B. Chacko, M. S. Johnson, V. M. Darley-Usmar, A review of the mitochondrial and glycolytic metabolism in human platelets and leukocytes: Implications for their use as bioenergetic biomarkers. *Redox Biol.* **2**, 206–210 (2014).
36. M. Rupnick, D. Panigrahy, C.-Y. Zhang, S. M. Dallabrida, B. B. Lowell, R. Langer, M. J. Folkman, Adipose tissue mass can be regulated through the vasculature. *Proc. Natl. Acad. Sci. U.S.A.* **99**, 10730–10735 (2002).
37. E. Bråkenhielm, R. Cao, B. Gao, B. Angelin, B. Cannon, P. Parini, Y. Cao, Angiogenesis inhibitor, TNP-470, prevents diet-induced and genetic obesity in mice. *Circ. Res.* **94**, 1579–1588 (2004).
38. Y. M. Kim, J. J. An, Y.-J. Jin, Y. Rhee, B. S. Cha, H. C. Lee, S.-K. Lim, Assessment of the anti-obesity effects of the TNP-470 analog, CKD-732. *J. Mol. Endocrinol.* **38**, 455–465 (2007).
39. J. Tam, D. G. Duda, J. Y. Perentes, R. S. Quadri, D. Fukumura, R. K. Jain, Blockade of VEGFR2 and not VEGFR1 can limit diet-induced fat tissue expansion: Role of local versus bone marrow-derived endothelial cells. *PLOS ONE* **4**, e4974 (2009).
40. Y. Cao, Adipose tissue angiogenesis as a therapeutic target for obesity and metabolic diseases. *Nat. Rev. Drug Discov.* **9**, 107–115 (2010).
41. Y. Cao, Angiogenesis modulates adipogenesis and obesity. *J. Clin. Invest.* **117**, 2362–2368 (2007).
42. M. E. Rausch, S. Weisberg, P. Vardhana, D. V. Tortoriello, Obesity in C57BL/6J mice is characterized by adipose tissue hypoxia and cytotoxic T-cell infiltration. *Int. J. Obes.* **32**, 451–463 (2008).
43. N. Hosogai, A. Fukuhara, K. Oshima, Y. Miyata, S. Tanaka, K. Segawa, S. Furukawa, Y. Tochino, R. Komuro, M. Matsuda, I. Shimomura, Adipose tissue hypoxia in obesity and its impact on adipocytokine dysregulation. *Diabetes* **56**, 901–911 (2007).
44. J. Ye, Z. Gao, J. Yin, Q. He, Hypoxia is a potential risk factor for chronic inflammation and adiponectin reduction in adipose tissue of *ob/ob* and dietary obese mice. *Am. J. Physiol. Endocrinol. Metab.* **293**, E1118–E1128 (2007).
45. K. Sun, C. M. Kusminski, P. E. Scherer, Adipose tissue remodeling and obesity. *J. Clin. Invest.* **121**, 2094–2101 (2011).
46. M. Bagchi, L. A. Kim, J. Boucher, T. E. Walshe, C. R. Kahn, P. A. D'Amore, Vascular endothelial growth factor is important for brown adipose tissue development and maintenance. *FASEB J.* **27**, 3257–3271 (2013).
47. Z. Belaid, F. Hubint, C. Humblet, J. Boniver, B. Nusgens, M. P. Defresne, Differential expression of vascular endothelial growth factor and its receptors in hematopoietic and fatty bone marrow: Evidence that neuropilin-1 is produced by fat cells. *Haematologica* **90**, 400–401 (2005).
48. S. S. Ghode, M. S. Bajaj, R. S. Kulkarni, L. S. Limaye, Y. S. Shouche, V. P. Kale, Neuropilin-1 is an important niche component and exerts context-dependent effects on hematopoietic stem cells. *Stem Cells Dev.* **26**, 35–48 (2017).
49. C. L. Abram, G. L. Roberge, Y. Hu, C. A. Lowell, Comparative analysis of the efficiency and specificity of myeloid-Cre deleting strains using ROSA-EYFP reporter mice. *J. Immunol. Methods* **408**, 89–100 (2014).
50. N. Ruderman, D. Chisholm, X. Pi-Sunyer, S. Schneider, The metabolically obese, normal-weight individual revisited. *Diabetes* **47**, 699–713 (1998).

Acknowledgments: We thank M. Buscarlet for running RNA-seq experiments and R. Chidiac for assistance with GSEA. We thank M. Dupuis at the Maisonneuve-Rosemont Hospital cytometry platform for cell-sorting experiments. We thank the Centre de recherche du Centre hospitalier de l'Université de Montréal (CRCHUM) metabolic platform and E. Joly and J. Lamontagne for performing functional metabolic analysis. Metabolic chamber experiments were performed by the platform of M. Kokoeva at the McGill University Health Centre (MUHC) with the assistance of X. Liu. This work benefited from data assembled by the ImmGen consortium (*18*). **Funding:** A.M.W. holds a fellowship from the Natural Sciences and Engineering Research Council of Canada (NSERC) (PDF-471745-2015). This work was supported by operating grants to P.S. from the Canadian Institutes of Health Research (CIHR) (324573 and 221478), the Heart and Stroke Foundation (G-16-00014658), the Foundation Fighting Blindness (FFB) Canada, the Canadian Diabetes Association (OG-3-11-3329-PS), and NSERC (418637). P.S. holds the Wolfe Professorship in Translational Research and a Canada Research Chair in Retinal Cell Biology. J.-S.J. is supported by the Burroughs Wellcome Fund Career Award for Medical Scientists, FFB, Fonds de recherche du Québec–Santé (FRQS), CIHR, and NSERC. M.M. is supported by Le Fonds de recherche du Québec, Consortium québécois sur la découverte du médicament, and NSERC. **Author contributions:** A.M.W., Z.S., and P.S. conceived the study, designed experiments, and wrote the manuscript. A.M.W., Z.S., V.G., G.M., J.-F.D., A.D., F.P., N.P., S.B., C.P., M.O., and V.d.G. performed experiments. A.M.W. and Z.S. interpreted results and generated figures. A.M.W., Z.S., and V.G. carried out the statistical analyses. P.S., M.M., F.S., M.L., N.L., G.L., and J.-S.J. provided feedback and supervised aspects of the study. P.S. supervised the overall implementation of the study. **Competing interests:** The authors declare that they have no competing interests. **Data and materials availability:** RNA-seq data is available at GEO under accession number GSE110447.

Submitted 18 April 2017
Accepted 18 January 2018
Published 16 March 2018
10.1126/sciimmunol.aan4626

Citation: A. M. Wilson, Z. Shao, V. Grenier, G. Mawambo, J.-F. Daudelin, A. Dejda, F. Pilon, N. Popovic, S. Boulet, C. Parinot, M. Oubaha, N. Labrecque, V. de Guire, M. Laplante, G. Lettre, F. Sennlaub, J.-S. Joyal, M. Meunier, P. Sapieha, Neuropilin-1 expression in adipose tissue macrophages protects against obesity and metabolic syndrome. *Sci. Immunol.* **3**, eaan4626 (2018).

Science Immunology

Neuropilin-1 expression in adipose tissue macrophages protects against obesity and metabolic syndrome

Ariel Molly Wilson, Zhuo Shao, Vanessa Grenier, Gaëlle Mawambo, Jean-François Daudelin, Agnieszka Dejda, Frédérique Pilon, Natalija Popovic, Salix Boulet, Célia Parinot, Malika Oubaha, Nathalie Labrecque, Vincent de Guire, Mathieu Laplante, Guillaume Lettre, Florian Sennlaub, Jean-Sebastien Joyal, Michel Meunier and Przemyslaw Sapieha

Sci. Immunol. **3**, eaan4626.
DOI: 10.1126/sciimmunol.aan4626

Keeping the calm in the adipose tissue

Obesity is associated with chronic inflammation and accumulation of immune cells in adipose tissue. Here, Wilson *et al*. report that macrophages that express neuropilin-1 (NRP1) play an essential role in limiting obesity-associated inflammation. In mice placed on a high-fat diet, deletion of NRP1 in myeloid cells accelerated both weight gain and development of insulin resistance. The authors found that NRP1 regulated fatty acid uptake in macrophages and that deficiency of NRP1 skewed their metabolism toward glycolysis, which is associated with a more aggressive inflammation. The studies add to the growing recognition of the importance of immune cells in obesity and other metabolic syndromes.